Magnetic Cyanide Tape

Deutsche Ausgabe: DOI: 10.1002/ange.201410664
Internationale Ausgabe: DOI: 10.1002/anie.201410664

A Single-Chain Magnet Tape Based on Hexacyanomanganate(III)**

Yuan-Zhu Zhang, Han-Hua Zhao, Edward Funck, and Kim R. Dunbar**

Abstract: *The tape-like chain* $\{[(tptz)Mn^{II}(H_2O)\text{-}Mn^{III}(CN)_6]_2Mn^{II}(H_2O)_2\}_n \cdot 4n\,MeOH \cdot 2n\,H_2O$ *based on the anisotropic building block hexacyanomanganate(III) exhibits long-range magnetic ordering below 5.1 K as well as single-chain magnetic behavior at lower temperatures with an effective energy barrier of 40.5(7) K.*

One-dimensional (1D) transition-metal coordination polymers are interesting materials that often exhibit unusual behavior that is intermediate between the molecular and bulk regimes.[1] Examples of chain architectures include ladders, ropes, and cluster-based 1D systems.[2] After years of being less studied in favor of higher-dimensionality conductors and magnets, the discovery of the first example of nanomolecular wires in 2001,[3] with the evocative name of single-chain magnets (SCMs) being introduced in 2002,[4] stimulated a renaissance of research on the topic of chain compounds. SCMs exhibit slow relaxation of the magnetization at low temperatures and may have potential applications in high-density information storage.[5] A variety of SCMs have been realized by implemention of astute design approaches involving the selection of specific bridging units in combination with anisotropic metal ion mononuclear or polynuclear complexes with ancillary ligands.[5] Among the known SCMs are those based on cyanometallate anions, which constitute a convenient platform for the isolation of structurally related materials by using a building-block or modular synthetic approach.[6,7] The first reported cyanide-bridged SCM is $\{[Fe^{III}(L)(CN)_4]_2Co^{II}(H_2O)_2\}\cdot 4H_2O$ (L = 2,2′-bipyridine or 1,10-phenanthroline), which consists of neutral cyanide-bridged Fe^{III}-Co^{II} double zigzag chains,[6e] or the so-called 4,2-ribbon chain.[2a] This architecture is a common structural archetype for SCMs and photo-responsive SCMs, which is most likely due to the favorable parallel arrangement of the anisotropic metal units.[6,8] Expanding this structural type to a tape is one of the challenges in this area that piqued our interest.[2b,7m]

In contrast to the other hexacyanometallate building blocks of the 3d elements, the $[Mn^{III}(CN)_6]^{3-}$ anion remains much less explored due to its inherent instability involving cyanide loss in the absence of free cyanide.[9,7c] This anion is quite intriguing because of the presence of unquenched orbital angular momentum originating from first-order spin–orbit coupling of the low-spin (LS) t_{2g}^4 Mn^{III} ion, which endows it with significant single-ion anisotropy. This anionic building block is a promising candidate for both SMMs and SCMs, provided the chemistry can be controlled. In 2003, our group isolated one of the first cyanide SMM ($[Mn^{II}_3Mn^{III}_2]$), which is a trigonal bipyramidal pentanuclear cluster with $[Mn(CN)_6]^{3-}$ anions occupying the axial positions.[10] Theoretical studies based on this compound led to the prediction that a linear trinuclear molecule containing the Mn^{II}–NC–Mn^{III}–CN–Mn^{II} unit should exhibit an SMM barrier height larger than 100 K, a hypothesis that has yet to be tested.[11]

Given the aforementioned findings, we recently turned our attention to the elaboration of 1D chains based on the $[Mn(CN)_6]^{3-}$ building block. We initiated this work by targeting the use of the centrosymmetric linear trinuclear compound $[(tptz)_2Mn^{II}_3(OAc)_6]$ (**1**, tptz = 2,4,6-tri(2-pyridyl)-1,3,5-triazine), which contains two different environments for the Mn^{II} ions.[12] We postulated that the labile acetate bridging ligands could be replaced with $[Mn(CN)_6]^{3-}$ anions, and that the chelating tptz ligands would serve to prevent the extension of the structure to a two-dimensional layered motif (Scheme 1). Indeed, slow diffusion of $\{[18\text{-C-6 K}]_3[Mn(CN)_6]$ into **1** affords the unusual compound $\{[(tptz)Mn^{II}(H_2O)\text{-}Mn^{III}(CN)_6]_2Mn^{II}(H_2O)_2\}_n \cdot 4n\,MeOH \cdot 2n\,H_2O$ (**2**) with a tape-like chain structure. Magnetic studies revealed that **2** exhibits long-range magnetic ordering below 5.1 K that is due to both intra- and inter-chain antiferromagnetic couplings as well as SCM behavior at lower temperatures with an effective energy barrier of 40.5(7) K.

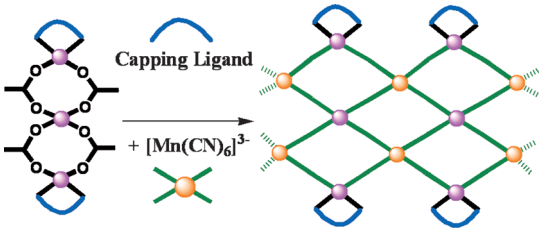

Scheme 1. Representation of the chain formation after substitution of the acetates in **1** by hexacyanomanganate(III).

Single-crystal X-ray diffraction studies revealed that both **1** and **2** crystallize in the triclinic $P\bar{1}$ space group. The structure of **1** contains a centrosymmetric linear trinuclear unit in which the central octahedral Mn2 atom is bridged by six acetate ligands to the terminal heptacoordinate Mn1 and Mn1 A atoms (Figure 1 a). The Mn2 center is in a compressed octahedral $[MnO_6]$ environment, with six oxygen atoms from the acetate ligands; the axial bonds (Mn2–O1/O1A 2.108(2) Å) are slightly shorter than those in the equatorial

[*] Dr. Y.-Z. Zhang, Dr. H.-H. Zhao, E. Funck, Prof. Dr. K. R. Dunbar
Department of Chemistry, Texas A&M University
College Station, TX 77842 (USA)
E-mail: hanhua@chem.tamu.edu
Dunbar@chem.tamu.edu
Homepage: http://www.chem.tamu.edu/rgroup/dunbar/

[**] This project was granted financial support from the Department of Energy (DE-FG02-02ER45999). Funds for the SQUID magnetometer were obtained from the National Science Foundation.

Supporting information for this article is available on the WWW under http://dx.doi.org/10.1002/anie.201410664.

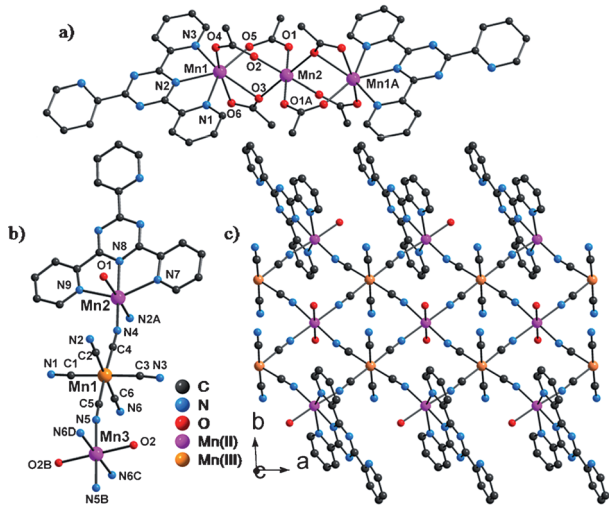

Figure 1. a) X-ray structure of **1**. b) The asymmetric unit of **2**. c) The tape architecture of **2** composed of fused zig-zag chains. All hydrogen atoms and interstitial solvent molecules are omitted for clarity.

plane (2.212(2) and 2.246(2) Å). The Mn1 ion adopts a distorted pentagonal bipyramidal geometry with O4 and O6 in the axial positions and tptz serving as a tridentate chelating ligand in the equatorial plane. Two of the acetate groups act as 2.11 (*syn–syn*)[13] bridges between Mn2 and Mn1, whereas the third exhibits the 3.21 (μ_2-O,O,O′) bridging mode with a Mn1–O3–Mn2 angle of 107.68(9)°. The intramolecular Mn···Mn distance is 3.81(2) Å.

The structure of **2** is best described as a tape consisting of quadruply cyanide-bridged Mn^{III}–Mn^{II} zig-zag chains or double 4,2-ribbons along the *a* axis (Figure 1c). Each Mn^{III} center in the $[Mn^{III}(CN)_6]^{3-}$ anions is in a slightly distorted octahedral geometry with Mn–C distances of 1.950(2)–2.011(2) Å and C-Mn-C angles in the range 86.9(4)–93.7(5)°. There are two different Mn^{II} ions: Mn2 resides in a distorted octahedral geometry with one chelating tptz ligand, two coordinated $[Mn^{III}(CN)_6]^{3-}$ units in a *cis* disposition, and a bound water molecule. The *cis* N-Mn-N angles vary from 70.56(11) to 110.53(38)°. The octahedral Mn3 ion is located on an inversion center and linked by four $[Mn^{III}(CN)_6]^{3-}$ anions in the equatorial plane with Mn–$N_{cyanide}$ 2.197(35)–2.230(34) Å; two water molecules occupy the axial positions (Mn–O 2.204(36) Å; Figure 1b). Each $[Mn^{III}(CN)_6]^{3-}$ anion is linked to two Mn2 and two Mn3 atoms through cyanide bridges in the equatorial positions while each Mn2 and Mn3 is connected to two $[Mn^{III}(CN)_6]^{3-}$ anions to form a 4,2-ribbon chain along the *a* axis, which is further expanded by sharing the Mn3 atoms to form a tape. The cyanide linkages deviate slightly from linearity with the Mn^{III}-C-N and Mn-N-C angles being in the ranges 175.4(4)–179.0(5)° and 168.5(3)–171.4(4)°, respectively. The nearest intrachain Mn–Mn separations are in the range of 5.24(8) to 5.33(5) Å. The chains interact to form a three-dimensional structure by π–π stacking interactions between the tptz ligands as well as hydrogen bonding (Supporting Information, Figure S1).

Magnetic susceptibility data for **1** and **2** were measured over the temperature range of 2–300 K under a direct current (dc) field of 1 kOe. The $\chi_m T$ value of 1 at 300 K (calculated for the $[Mn^{II}_3]$ unit) is 12.85 $cm^3 mol^{-1} K$, which is consistent with the spin-only value (13.125 $cm^3 mol^{-1} K$) for three isolated high-spin (HS) Mn^{II} ions (Supporting Information, Figure S2). Based on the Hamiltonian: $H = -2J(S_{Mn1}S_{Mn2} + S_{Mn2}S_{Mn1A})$, ($S_{Mn} = 5/2$), J is the magnetic interaction between the Mn ions), the best fit to the data using the PHI program[14] led to the values $g = 2.01$ and $J = -0.81$ cm^{-1}, an indication of very weak antiferromagnetic (AF) coupling between the Mn ions. The isothermal magnetization (M) as a function of the field (H) measured at 1.9 K reaches the value of about 5.0 Nβ between 20–30 kOe, and then increases steeply at higher fields. These data are in accord with the conclusion that the weak AF interaction between the Mn ions results in a ferrimagnetic state ($S = 5/2$, $M = 5.0$ Nβ), which is easily overcome at higher applied fields. The best fit for the M–H data gave $J = -0.78$ cm^{-1} and $g = 2.01$, consistent with the parameters extracted from the M–T data (Supporting Information, Figure S2, inset).

The plot of $\chi_m T$ versus T for **2** is indicative of typical ferrimagnetic behavior as a result of the non-compensating moments of the AF-coupled Mn^{II} and Mn^{III} ions (Figure 2).

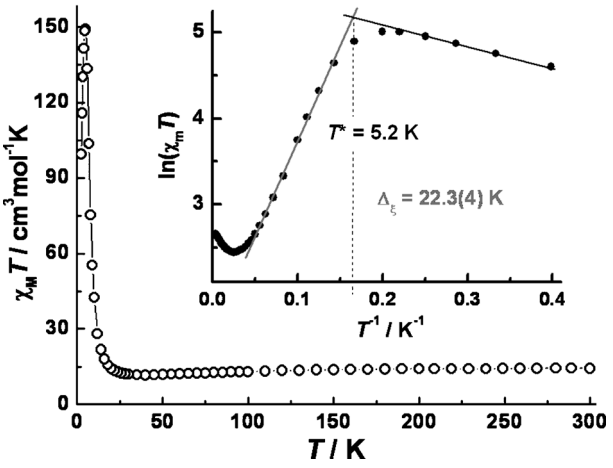

Figure 2. Variable-temperature dc magnetic susceptibility data for **2**, measured in an applied field of 1 kOe. Inset: Plot of $\ln(\chi_m T)$ *vs* $1/T$.

The $\chi_m T$ value of 14.26 $cm^3 mol^{-1} K$ at 300 K is lower than the expected spin-only value of 15.13 $cm^3 mol^{-1} K$ for three HS Mn^{II} ($S = 5/2$) and two LS Mn^{III} ($S = 1$) ions (calculated for the $[Mn^{II}_3Mn^{III}_2]$ unit), which is most likely due to the spin–orbital coupling effects of the Mn^{III} ions. The $\chi_m T$ value decreases gradually to a minimum of 11.56 $cm^3 mol^{-1} K$ at 40 K and then increases sharply to a maximum of 149.1 $cm^3 mol^{-1} K$ at 5.0 K. The further sharp decrease below 5 K is attributed to interchain AF coupling and/or zero-field splitting (ZFS). A fitting of the data above 40 K to the Curie–Weiss law gives a C value of 15.05 $cm^3 mol^{-1} K$ and a negative θ constant of −15.6 K (Supporting Information, Figure S3). No suitable modelling for further analysis of the data was attempted because of the complicated topology.

The isothermal field-dependent magnetization (M *vs* H) was measured at 1.8 K (Supporting Information, Figure S4).

In the very low-field region, the magnetization curve for **2** exhibits a sigmoidal shape, typical of a field-induced metamagnetic transition at a critical field of 200 Oe. After the transition, the magnetization increases rapidly but does not fully saturate even at 7 T, as the value of 9.27 Nβ is lower than the estimation of 11.0 Nβ per $[Mn^{II}_3Mn^{III}_2]$ for a g of **2**. These data indicate the presence of significant magnetic anisotropy. It should be mentioned that **2** exhibits a negligible hysteresis loop (Supporting Information, Figure S5). Field-cooled magnetizations (FCMs) at different dc fields further confirmed the metamagnetism of **2** (Supporting Information, Figure S6). The FCMs at below 200 Oe display a peak at around 5 K, which disappears at higher fields, indicating the transition from an AF state to paramagnetic state.

For an anisotropic Heisenberg or Ising-like one-dimensional system, $\chi_m T$ increases exponentially with decreasing temperature, and follows the equation: $\chi_m T/C_{eff} = \exp(\Delta_\xi/k_B T)$, where C_{eff} is the effective Curie constant, Δ_ξ is the correlation energy (the energy needed to create a domain wall in the chain), and k_B is the Boltzmann constant. In fact, the resulting plot of $\ln(\chi_m T)$ versus $1/T$ for **2** features a linear region in the temperature range 7–20 K, yielding $\Delta_\xi = 22.3(4)$ K, suggesting SCM characteristics (Figure 2, inset). Below 7 K, $\ln(\chi_m T)$ reaches a maximum and then undergoes a linear decrease at lower temperatures. The crossover temperature T^* is about 5.2 K extracted from the intersection of the two linear regimes.

To verify SCM behavior for **2**, alternating current (ac) magnetic susceptibility measurements were performed as a function of both temperature and frequency in a 5 Oe ac field and a zero dc magnetic field. Figure 3 clearly reveals that variable-temperature ac susceptibility measurements for **2** exhibit peaks for the in-phase but no signals for an out-of-phase component at 5.1 K due to the long-range AF ordering. In sharp contrast, at lower temperatures (below 4 K), strong frequency dependence of both in-phase (χ_m') and out-of-phase (χ_m'') components is evident. The relaxation times, extracted from the peaks of χ_m'', were plotted as $\ln(\tau)$ *vs* T^{-1}, following an Arrhenius law $\tau = \tau_0 \exp(\Delta_\tau/k_B T)$ with $\Delta_\tau/k_B = 40.5(7)$ K and $\tau_0 = 1.0(3) \times 10^{-11}$ s (Figure 3, inset). The results are in good agreement with those reported for other SCMs.[5] Given that the dynamics of the magnetization occur below the crossover temperature (5.2 K), the slow relaxation is considered to be within the finite-size regime, where the overall spin-reversal barrier can be expressed as the sum of the correlation and anisotropy energies, $\Delta_\tau = \Delta_\xi + \Delta_A$.[15] Thus, Δ_A may be estimated as 18.2 K. It should be mentioned that the recent finding of magnet behavior in AF ordered phases of SCMs by Coulon, Clérac et al. in 2009[16] have prompted a new approach for SCMs and the field is expanding as different examples of these fascinating systems continue to be developed.[17] What is more, ferromagnetic interchain interactions of SCMs may lead to a three-dimensional ordering magnet with significantly enhanced coercivity.[18]

Variable-frequency ac susceptibilities collected over the temperature range 1.80–2.70 K also show highly frequency-dependent peaks (Figure 4a). As above, the relaxation time

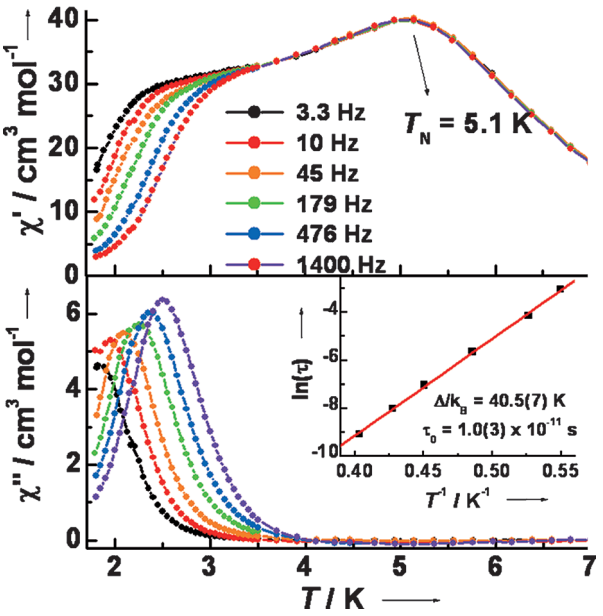

Figure 3. Variable-temperature in-phase (top) and out-of-phase (bottom) components of the ac magnetic susceptibility data for **2**, collected in a 5 Oe ac field oscillating at frequencies of 3.3–1400 Hz. Inset: Arrhenius plot of relaxation times.

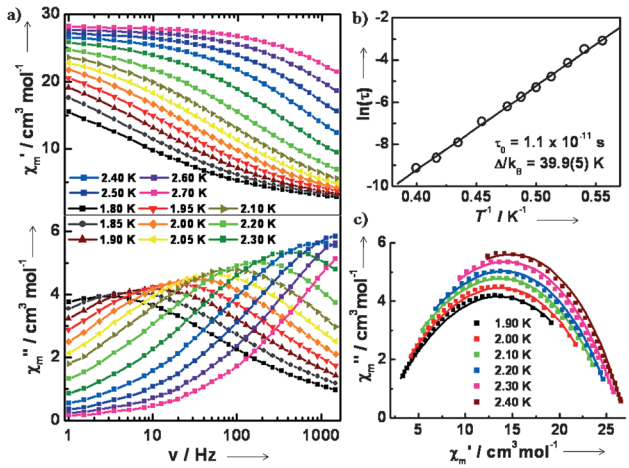

Figure 4. a) Variable-frequency in-phase (χ_m') and out-of-phase (χ_m'') ac magnetic susceptibility data, collected in zero dc applied field and a 5 Oe oscillating ac field at temperatures from 1.80 to 2.70 K. b) Arrhenius plot of relaxation times. c) Cole–Cole plots.

follows an Arrhenius law with $\Delta/k_B = 39.9(5)$ K, $\tau_0 = 1.1(2) \times 10^{-11}$ s, consistent with the values reported above (Figure 4b). Cole–Cole plots (Figure 4c; Supporting Information, Table S1) of χ_m' vs. χ_m'' were fitted to a generalized Debye model,[19] which led to α values ranging from 0.49 to 0.57, indicative of a relatively wide distribution of relaxation times, which may be caused by the variable distributions in chain length, magnetic interchain interactions, and random defects as found in other cases where α ranges from 0–0.7.[5c]

It has been found for three-dimensional AF ordered phases of SCMs that "pure" SCM behavior may be observed when a small dc field being applied, which may minimize the

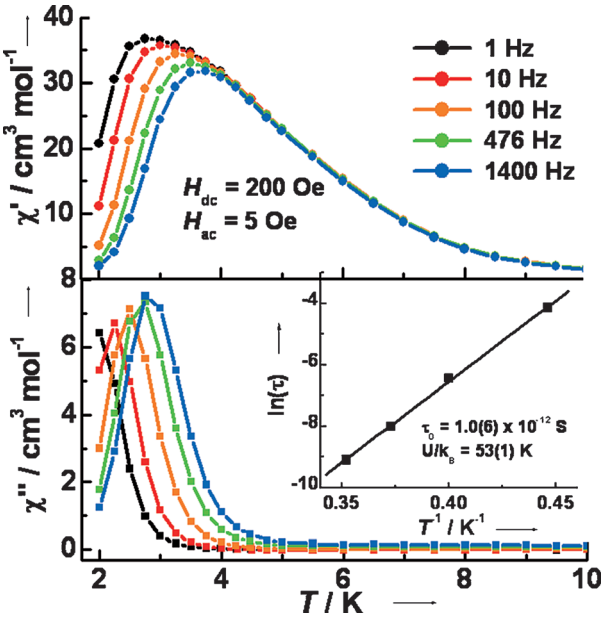

Figure 5. Variable-temperature in-phase (top) and out-of-phase (bottom) components of the ac magnetic susceptibility data for **2**, collected in a 5 Oe ac field and 200 Oe of dc field oscillating at frequencies of 1–1400 Hz. Inset: Arrhenius plot of relaxation times.

effect of the AF interchain interaction and slow down the observed dynamics.[17] In this regard, additional variable-temperature ac susceptibilities were measured under applied dc fields of 50 Oe and 200 Oe. As a result, the AF ordering temperature decreased to 4.9 K under a dc field of 50 Oe (Supporting Information, Figure S7) and totally disappeared under 200 Oe (Figure 5). The relaxation time extracted from Figure 5 follows an Arrhenius law with $\Delta/k_B = 53(1)$ K and $\tau_0 = 1.0(6) \times 10^{-12}$ s.

In summary, a unique tape-like cyanide-bridged chain compound (**2**) has been prepared with the anisotropic $[Mn^{III}(CN)_6]^{3-}$ anion. Compound **2** exhibits long-range antiferromagnetic ordering with a Néel temperature of 5.1 K due to both intra- and inter-chain AF coupling between the metal spin centers. An unusual feature of the magnetism is that SCM behavior is clearly evidenced at lower temperatures with an effective energy barrier of 40.5(7) K. Efforts to minimize the interchain interactions and extend this chain architecture to other cyanide building blocks are underway.

Experimental Section

Synthesis of **1**: A MeOH (10 mL) solution of tptz (248 mg, 0.79 mmol) was added dropwise into a solution of $Mn(OAc)_2{\cdot}4H_2O$ (294 mg, 1.20 mmol) in MeOH (10 mL) with stirring to give a clear yellow solution which was stirred for 3 h and then concentrated to about 5 mL on a rotary evaporator. A light yellow solid was obtained by adding diethyl ether. The powder was collected by filtration, washed with MeOH, and dried in vacuo, yield: 256 mg (56 %). Single crystals of **1** were grown by slow diffusion of diethyl ether into a solution of 20 mg of **1** in methanol (2 mL). Anal. calcd. for $C_{48}H_{44}Mn_3N_{12}O_{13}$: N 14.47, C 49.62, H 3.82; found: N 14.64, C 49.11, H 3.59 %.

Synthesis of **2**: A sample of **1** (12.0 mg, 0.0105 mmol) dissolved in MeOH (1.5 mL) was carefully layered over a MeOH–DMF (1.5 mL, v/v = 2:1) solution of 22.5 mg (0.0201 mmol) of $[(18\text{-crown-}6)K]_3Mn(CN)_6$ in a 6 mm diameter tube, which was sealed under a reduced nitrogen pressure. Brown crystals were obtained after two weeks and collected by filtration, washed with small amount of MeOH, and dried in air. Yield: 9.0 mg (62 %). IR (Nujol): $\nu \sim = 2138$, 2130 cm^{-1} for cyanide stretches.

Crystal data for **1**: $C_{48}H_{42}Mn_3N_{12}O_{12}$, $M_w = 1143.76\ g\,mol^{-1}$, triclinic, space group $P\bar{1}$, $a = 8.4873(17)$, $b = 11.710(2)$, $c = 13.099(3)$ Å, $\alpha = 98.891(12)$, $\beta = 104.418(11)$, $\gamma = 104.768(11)°$, $V = 1185.7(4)$ Å^3, $Z = 1$, $\mu = 7.073\ mm^{-1}$, $\rho_{calcd} = 1.602\ Mg\,m^{-3}$, $R_1 = 0.0456$, $wR_2 = 0.1131$.

Crystal data for **2**: $C_{52}H_{52}Mn_5N_{24}O_{10}$, $M_w = 1447.88\ g\,mol^{-1}$, triclinic, space group $P\bar{1}$, $a = 7.5739(15)$, $b = 14.164(3)$, $c = 14.996(3)$ Å, $\alpha = 99.39(3)$, $\beta = 90.35(3)$, $\gamma = 92.81(3)°$, $V = 1585.1(5)$ Å^3, $Z = 1$, $\mu = 1.043\ mm^{-1}$, $\rho_{calcd} = 1.517\ Mg\,m^{-3}$, $R_1 = 0.0814$, $wR_2 = 0.1944$.

CCDC 1021129 (**1**) and CCDC 965506 (**2**) contain the supplementary crystallographic data for this paper. These data can be obtained free of charge from The Cambridge Crystallographic Data Centre via www.ccdc.cam.ac.uk/data_request/cif.

Keywords: hexacyanomanganate · long-range order · magnetic tape · single-chain magnets

How to cite: *Angew. Chem. Int. Ed.* **2015**, *54*, 5583–5587
Angew. Chem. **2015**, *127*, 5675–5679

[1] a) C.-T. Chen, K. S. Suslick, *Coord. Chem. Rev.* **1993**, *128*, 293–322; b) W. L. Leong, J. J. Vittal, *Chem. Rev.* **2011**, *111*, 688–764.

[2] a) J. Cernák, M. Orendac, I. Potocnak, J. Chomic, A. Orendacova, J. Skorsepa, A. Feher, *Coord. Chem. Rev.* **2002**, *224*, 51–66; b) Y.-Z. Zhang, H.-Y. Wei, F. Pan, Z.-M. Wang, Z.-D. Chen, S. Gao, *Angew. Chem. Int. Ed.* **2005**, *44*, 5841–5846; *Angew. Chem.* **2005**, *117*, 5991–5996; c) R. Podgajny, R. Pełka, C. d. Desplanches, L. Ducasse, W. Nitek, T. Korzeniak, O. Stefanczyk, M. Rams, B. Sieklucka, M. Verdaguer, *Inorg. Chem.* **2011**, *50*, 3213–3222; d) M. Shatruk, K. E. Chambers, A. V. Prosvirin, K. R. Dunbar, *Inorg. Chem.* **2007**, *46*, 5155–5165; e) R. Lescouëzec, J. Vaissermann, L. M. Toma, R. Carrasco, F. Lloret, M. Julve, *Inorg. Chem.* **2004**, *43*, 2234–2236; f) J. L. Heinrich, J. J. Sokol, A. G. Hee, J. R. Long, *J. Solid State Chem.* **2001**, *159*, 293–301.

[3] A. Caneschi, D. Gatteschi, N. Lalioti, C. Sangregorio, R. Sessoli, G. Venturi, A. Vindigni, A. Rettori, M. G. Pini, M. A. Novak, *Angew. Chem. Int. Ed.* **2001**, *40*, 1760–1763; *Angew. Chem.* **2001**, *113*, 1810–1813.

[4] R. Clérac, H. Miyasaka, M. Yamashita, C. Coulon, *J. Am. Chem. Soc.* **2002**, *124*, 12837–12844.

[5] a) W.-X. Zhang, R. Ishikawa, B. Breedlove, M. Yamashita, *RSC Adv.* **2013**, *3*, 3772–3798; b) H. Miyasaka, M. Julve, M. Yamashita, R. Clerac, *Inorg. Chem.* **2009**, *48*, 3420–3437; c) H.-L. Sun, Z.-M. Wang, S. Gao, *Coord. Chem. Rev.* **2010**, *254*, 1081–1100.

[6] a) K. Mitsumoto, M. Ui, M. Nihei, H. Nishikawa, H. Oshio, *CrystEngComm* **2010**, *12*, 2697–2699; b) L. M. Toma, R. Lescouezec, S. Uriel, R. Llusar, C. Ruiz-Perez, J. Vaissermann, F. Lloret, M. Julve, *Dalton Trans.* **2007**, 3690–3698; c) L. M. Toma, R. Lescouezec, J. Pasan, C. Ruiz-Perez, J. Vaissermann, J. Cano, R. Carrasco, W. Wernsdorfer, F. Lloret, M. Julve, *J. Am. Chem. Soc.* **2006**, *128*, 4842–4853; d) S. Wang, J. L. Zuo, S. Gao, Y. Song, H. C. Zhou, Y. Z. Zhang, X. Z. You, *J. Am. Chem. Soc.* **2004**, *126*, 8900–8901; e) R. Lescouëzec, J. Vaissermann, C. Ruiz-Perez, F. Lloret, R. Carrasco, M. Julve, M. Verdaguer, Y. Dromzee, D. Gatteschi, W. Wernsdorfer, *Angew. Chem. Int. Ed.* **2003**, *42*, 1483–1486; *Angew. Chem.* **2003**, *115*, 1521–1524.

[7] a) X. Chen, S.-Q. Wu, A.-L. Cui, H.-Z. Kou, *Chem. Commun.* **2014**, *50*, 2120–2122; b) R. Ababei, C. Pichon, O. Roubeau, Y.-

G. Li, N. Bréfuel, L. Buisson, P. Guionneau, C. Mathonière, R. Clérac, *J. Am. Chem. Soc.* **2013**, *135*, 14840 – 14853; c) H. Miyasaka, T. Madanbashi, A. Saitoh, N. Motokawa, R. Ishikawa, M. Yamashita, S. Bahr, W. Wernsdorfer, R. Clerac, *Chem. Eur. J.* **2012**, *18*, 3942 – 3954; d) X. Feng, J. Liu, T. D. Harris, S. Hill, J. R. Long, *J. Am. Chem. Soc.* **2012**, *134*, 7521 – 7529; e) J. H. Yoon, D. W. Ryu, S. Y. Choi, H. C. Kim, E. K. Koh, J. Tao, C. S. Hong, *Chem. Commun.* **2011**, *47*, 10416 – 10418; f) X. Feng, T. David Harris, J. R. Long, *Chem. Sci.* **2011**, *2*, 1688 – 1694; g) N. Hoshino, Y. Sekine, M. Nihei, H. Oshio, *Chem. Commun.* **2010**, *46*, 6117 – 6119; h) T. D. Harris, M. V. Bennett, R. Clerac, J. R. Long, *J. Am. Chem. Soc.* **2010**, *132*, 3980 – 3988; i) J.-F. Guo, X.-T. Wang, B.-W. Wang, G.-C. Xu, S. Gao, L. Szeto, W.-T. Wong, W.-Y. Wong, T.-C. Lau, *Chem. Eur. J.* **2010**, *16*, 3524 – 3535; j) C. F. Wang, D. P. Li, X. Chen, X. M. Li, Y. Z. Li, J. L. Zuo, X. Z. You, *Chem. Commun.* **2009**, 6940 – 6942; k) D. Visinescu, A. M. Madalan, M. Andruh, C. Duhayon, J.-P. Sutter, L. Ungur, W. Van den Heuvel, L. F. Chibotaru, *Chem. Eur. J.* **2009**, *15*, 11808 – 11814; l) M. Ferbinteanu, H. Miyasaka, W. Wernsdorfer, K. Nakata, K. Sugiura, M. Yamashita, C. Coulon, R. Clerac, *J. Am. Chem. Soc.* **2005**, *127*, 3090 – 3099; m) L. M. Toma, R. Lescouezec, F. Lloret, M. Julve, J. Vaissermann, M. Verdaguer, *Chem. Commun.* **2003**, 1850 – 1851.

[8] a) D. P. Dong, T. Liu, S. Kanegawa, S. Kang, O. Sato, C. He, C. Y. Duan, *Angew. Chem. Int. Ed.* **2012**, *51*, 5119 – 5123; *Angew. Chem.* **2012**, *124*, 5209 – 5213; b) T. Liu, Y. J. Zhang, S. Kanegawa, O. Sato, *J. Am. Chem. Soc.* **2010**, *132*, 8250 – 8251.

[9] a) V. Hoeke, M. Heidemeier, E. Krickemeyer, A. Stammler, H. Bogge, J. Schnack, T. Glaser, *Dalton Trans.* **2012**, *41*, 12942 – 12959; b) V. Hoeke, K. Gieb, P. Muller, L. Ungur, L. F. Chibotaru, M. Heidemeier, E. Krickemeyer, A. Stammler, H. Bogge, C. Schroder, J. Schnack, T. Glaser, *Chem. Sci.* **2012**, *3*, 2868 – 2882; c) W. Kaneko, S. Kitagawa, M. Ohba, *J. Am. Chem. Soc.* **2007**, *129*, 248 – 249.

[10] C. P. Berlinguette, D. Vaughn, C. Canada-Vilalta, J. R. Galan-Mascaros, K. R. Dunbar, *Angew. Chem. Int. Ed.* **2003**, *42*, 1523 – 1526; *Angew. Chem.* **2003**, *115*, 1561 – 1564.

[11] a) S. I. Klokishner, S. M. Ostrovsky, A. V. Palii, K. Dunbar, *J. Mol. Struct.* **2007**, *838*, 144 – 150; b) A. Palii, S. M. Ostrovsky, S. I. Klokishner, B. S. Tsukerblat, K. R. Dunbar, *ChemPhysChem* **2006**, *7*, 871 – 879.

[12] A. Escuer, B. Cordero, X. Solans, M. Font-Bardia, T. Calvet, *Eur. J. Inorg. Chem.* **2008**, 5082 – 5087.

[13] X. Y. Wang, Z. M. Wang, S. Gao, *Chem. Commun.* **2008**, 281 – 294.

[14] N. F. Chilton, R. P. Anderson, L. D. Turner, A. Soncini, K. S. Murray, *J. Comput. Chem.* **2013**, *34*, 1164 – 1175.

[15] C. Coulon, H. Miyasaka, R. Clérac, *Struct. Bonding (Berlin)* **2006**, *122*, 163.

[16] C. Coulon, R. Clérac, W. Wernsdorfer, T. Colin, H. Miyasaka, *Phys. Rev. Lett.* **2009**, *102*, 167204.

[17] a) X.-M. Liu, B.-Y. Wang, W. Xue, L.-H. Xie, W.-X. Zhang, X.-N. Cheng, X.-M. Chen, *Dalton Trans.* **2012**, *41*, 13741 – 13746; b) J. Boeckmann, M. Wriedt, C. Näther, *Chem. Eur. J.* **2012**, *18*, 5284 – 5289; c) I. Bhowmick, E. A. Hillard, P. Dechambenoit, C. Coulon, T. D. Harris, R. Clerac, *Chem. Commun.* **2012**, *48*, 9717 – 9719; d) J. H. Yoon, J. W. Lee, D. W. Ryu, S. W. Yoon, B. J. Suh, H. C. Kim, C. S. Hong, *Chem. Eur. J.* **2011**, *17*, 3028 – 3034; e) H. Miyasaka, K. Takayama, A. Saitoh, S. Furukawa, M. Yamashita, R. Clérac, *Chem. Eur. J.* **2010**, *16*, 3656 – 3662; f) X.-J. Li, X.-Y. Wang, S. Gao, R. Cao, *Inorg. Chem.* **2006**, *45*, 1508 – 1516; g) D. Shao, S.-L. Zhang, X.-H. Zhao, X.-Y. Wang, *Chem. Commun.* **2015**, *51*, 4360 – 4363.

[18] a) R. Sessoli, *Angew. Chem. Int. Ed.* **2008**, *47*, 5508 – 5510; *Angew. Chem.* **2008**, *120*, 5590 – 5592; b) N. Ishii, Y. Okamura, S. Chiba, T. Nogami, T. Ishida, *J. Am. Chem. Soc.* **2008**, *130*, 24 – 25; c) H.-L. Sun, Z.-M. Wang, S. Gao, *Chem. Eur. J.* **2009**, *15*, 1757 – 1764.

[19] S. M. J. Aubin, Z. Sun, L. Pardi, J. Krzystek, K. Folting, L.-C. Brunel, A. L. Rheingold, G. Christou, D. N. Hendrickson, *Inorg. Chem.* **1999**, *38*, 5329 – 5340.

Received: November 1, 2014
Published online: March 17, 2015

